Clean Technologies and Recycling

Clean Technologies and Recycling, 2(3): 136–164.
DOI: 10.3934/ctr.2022008
Received: 21 April 2022
Revised: 26 July 2022
Accepted: 01 August 2022
Published: 12 August 2022

http://www.aimspress.com/journal/ctr

Research article

Compressive behavior of FRP-tube-confined concrete short columns using recycled FRP materials from wind turbine blades: Experimental investigation and analytical modelling

Dmitry Baturkin[1], Ousmane A. Hisseine[2], Radhouane Masmoudi[1,*], Arezki Tagnit-Hamou[1], Slimane Metiche[1] and Luc Massicotte[3]

[1] Department of Civil and Building Engineering, Université de Sherbrooke, Qc, Canada
[2] Department of Civil Engineering, McMaster University, ON, Canada
[3] Synergie-Matanie, Matane, Qc, Canada

* **Correspondence:** Email: radhouane.masmoudi@usherbrooke.ca.

Abstract: A major challenge in today's concrete construction is to lower its carbon footprint to the least possible level. This study provides insights on a new low-CO_2 alternative concrete whereby glass fiber-reinforced polymer (GFRP) materials from waste wind-turbine blades (WWTB)—termed as WWTB-GFRP—was utilized as: (i) replacement of Portland cement at 0%, 10%, 20%, and as (ii) lightweight aggregate replacement for natural aggregates at 0%, 50%, and 100%. The resulting WWTB-GFRP concretes were used in concrete-filled fibre-reinforced polymer (FRP) tubes (CFFTs) whereby the latter serves as a stay-in-place formwork and external reinforcement. Pristine WWTB-GFRP materials (containing wood) and processed ones (by wood removal) were investigated. Results indicate that while both WWTB-GFRP powder and aggregates adversely affect the compression resistance (due to, respectively, the retarding effect of the powder and the slippery surface of the aggregates leading to reduced bonding with the bulk cementitious matrix), the confinement of WWTB-GFRP concrete with FRP tubes offers an innovative tool to restore the strength loss. In fact, valorizing WWTB-GFRP concrete in CFFTs allowed to increase the compressive resistance by more than 100%. Interestingly, under axial compression, FRP tube confinement shifted the stress–strain response from the conventional brittle response to a ductile one whereby the confinement affected the elastic and plastic responses differently. While FRP confinement increased in the elastic limit at higher WWTB-GFRP aggregate content, it resulted in

lower slope of the plastic response at higher WWTB-GFRP aggregate content. An analytical assessment demonstrated that a WWTB-GFRP aggregate content of 55% will be optimum for enhancing both elastic and plastic responses. Building upon the ACI 440.2R-17 model for predicting the compressive response of confined concrete incorporating conventional aggregates, a modified model more sensitive to GFRP aggregates and with higher predictive ability was proposed. Research outcomes will contribute to recycling waste materials while endowing further sustainability to concrete.

Keywords: concrete-filled fibre-reinforced polymer tubes; glass fiber-reinforced polymer; low-CO_2 concrete; recycled aggregates; recycled materials; sustainable development; wind turbine blade waste materials

1. Introduction

Energy generation from clean sources such as Eolic energy has been pivotal in enabling the energy sector to embody sustainability imperatives as part of the global responsibility to support sustainable development. As such, wind power is expected to escalate in growth to supply up to 18% of the global electricity demand by 2050 [1]. Thus, in 2020 wind power supplied 16.4% of the electricity demand in the European Union (EU) and the United Kingdom [2] with the binding target for increasing the renewable energy share to 27% by 2030 and cutting greenhouse gas emissions by 80–95% by 2050 [3]. In Canada, over 3 million households are supplied by wind energy [4]. In the United States of America (USA), wind energy is expected to cover up to 35% of the nation's electricity demand by 2050 [5]. Whereas the majority of first installation wind turbine structures are tending to the end of their service life [4], the disposal of waste wind turbine blades represents an increasing environmental burden whereby landfilling remains (unfortunately) the most common waste management strategy. Although around 80% of the total weight of a wind turbine can be recycled including the tower, the gearbox, and the hub which contain large portions of steel [6], it is disappointing that blades are often landfilled [7].

Latest research in the EU highlighted four recycling methods for WWTB-GFRP materials: (i) mechanical grinding, (ii) fluidized bed, (iii) pyrolysis, and (iv) solvolysis, with mechanical grinding being the most effective for economical and environmental considerations [8].

One of the new avenues to recycle WWTB-GFRP is in concrete construction where the material is ground to fine powder to serve as a cement replacement. Material characterisation of GFRP powder by XRF proved the presence of SiO_2, a typical ingredient of glassy materials and a precursor of their reactivity with cementitious materials, which hints to the usefulness of incorporating WWTB-GFRP powder in concrete as partial cement replacement [9]. Asokan et al. [10,11] and Correia et al. [9] used mechanically ground GFRP powder as a substitution of fine aggregate in concrete. The increase in replacement rate was found to have an adverse effect on compressive and tensile strengths while leading to higher water demand to maintain the target workability.

In our recent investigation [12], whereas the use of WWTB-GFRP powder as a partial replacement of cement (at 10%, 20%, and 30%) led to drop in mechanical strength at 28 days, wood removal was found beneficial as it enabled attenuating the strength loss. In fact, the 90-day strength in WWTB-GFRP concrete (with 10% cement replacement) demonstrated strength comparable to that

of the reference concrete (the concrete without WWTB-GFRP) [12]. In the same study, we figured out that the drop in compressive strength is less in the case of replacement of natural aggregate with WWTB-GFRP aggregates, given that the retreading agent (wood) has less surface area even when the aggregates are used with their wooden content. Therefore, the valorization of WWTB-GFRP materials as aggregates in concrete has high potential to bring a twofold benefit: (i) waste management for GFRP industry [13], and (ii) an alternative to the abusive extraction of virgin concrete aggregates as highlighted at the international level due to the depletion of reserves of primary resources and the associated increasing environmental awareness [14]. It should be noted that the available literature indicates an obvious drop in compressive strength upon the incorporation of WWTB-GFRP materials: a drop of approximately 70% between when WWTB-GFRP aggregates was used at 0%, 50%, and 100% replacement of limestone aggregates [13,15]. In our recent study [12], we identified the wooden content in WWTB-GFRP as the major ingredient causing strength loss. Thus, removal of the wooden content mitigated the loss in mechanical strength and enabled attaining comparable strength by 90 days of curing. Nonetheless, it should be highlighted that WWTB-GFRP aggregates present another drawback. Owing to their slippery and smooth surfaces, WWTB-GFRP aggregates tend to split apart from the matrix upon axial loading. Additional to the lightweight of WWTB-GFRP aggregates, their slippery surfaces—not favoring adequate bond with the bulk cementitious matrix—further exacerbates the strength loss.

One possible solution to overcome the drawbacks of WWTB-GFRP aggregates on concrete mechanical performance could be the use of concrete-filled fiber-reinforced polymer (FRP) tubes (CFFTs) [16–20]. In this technology, a stay-in-place FRP formwork serves as external reinforcement to noticeably increase the compressive resistance of concrete and helps improving the durability of concrete structures under harsh environmental conditions [16]. The application of CFFT technology includes such structures as fender piles, dauphins, supports for marine structures, bridge pier protection, railway sleepers, external reinforcement by prefabricated FRP composite jackets can be used for structural repair [21–23]. The results of Boumarafy et al. (2015) [16] demonstrated a significant improvement in compressive strength for 152 × 300 mm CFFT short columns. The application of CFFT technology for concrete confinement was found to enhance the compressive strength of unconfined concrete by up to 2.16 times. The results of El-Zefzafy et al. (2013) [20] also demonstrated that confinement of short columns using CFFTs enables an increase in compressive strength exceeding 150% for confined cylinders compared to unconfined cylinders [20]. Several studies were found on recycled aggregate concrete from different origins confined with FRP tubes [24–27]. However, to the knowledge of the authors, this study stands out to be first to leverage FRP tube technology for valorizing recycled WWTB-GFRP materials as aggregate or as cement replacement in structural applications.

Therefore, this study is attempting to answer the following question: Bearing in mind the mechanical strength deficiency of WWTB-GFRP concrete, and in light of the phenomenal strength enhancing effect of CFFTs, can the valorization of WWTB-GFRP concrete in CFFTs enable overcoming the drawbacks of WWTB-GFRP concrete? To this end and following our recent investigation on WWTB-GFRP concrete [12], this study is intended to apply CFFTs to valorize WWTB-GFRP materials in two perspectives: as (i) cement replacement, and (ii) lightweight aggregates. Cement replacement by WWTB-GFRP powder at rates of 10% and 20% were attempted, while natural coarse aggregate replacement by WWTB-GFRP aggregates at levels of 50% and 100% were considered. In both cases, WWTB-GFRP concrete was evaluated in pristine condition as well

as after wood removal. The compression behavior of resulting concrete formulations was assessed on short columns of 152 × 300 mm using a 5000 kN MTS actuator. As the demand for cleaner energy increases, the waste management of FRP materials from wind turbine blades will continue to shape an environmental burden. The current research will contribute to alleviating that burden by identifying new recycling avenues for such waste materials while contributing to making greener concretes. Thus, research outcomes are expected to contribute to the ongoing progress in the development of greener materials for a sustainable built environment through recycling waste materials from industrial processes, thereby fostering the sustainable development.

2. Experimental program

2.1. Materials properties

2.1.1. Wind turbine blade waste material

The recycled WWTB-GFRP material (Figure 1) used in the project was received from the (QC, Canada). The material is obtained from disassembled wind turbines at the end of their service life. Part of the material was chipped using an industrial woodchipper of high processing capacity. Our previous study involved a comprehensive material characterisation [12]. The results are as follows: (i) WWTB-GFRP material consists of 64% glass fiber, 29% epoxy resin, and 7% wood by weight; (ii) The glass fiber in WWTB-GFRP consists of 55% SiO_2, 23% CaO, and 14% Al_2O_3; (iii) The average density of WWTB-GFRP powder is 1.66 g/cm^3, (iv) The density of WWTB-GFRP aggregates with wood content is 0.680 g/cm^3, and (v) The density of WWTB-GFRP aggregate without wood is 1.7 g/cm^3.

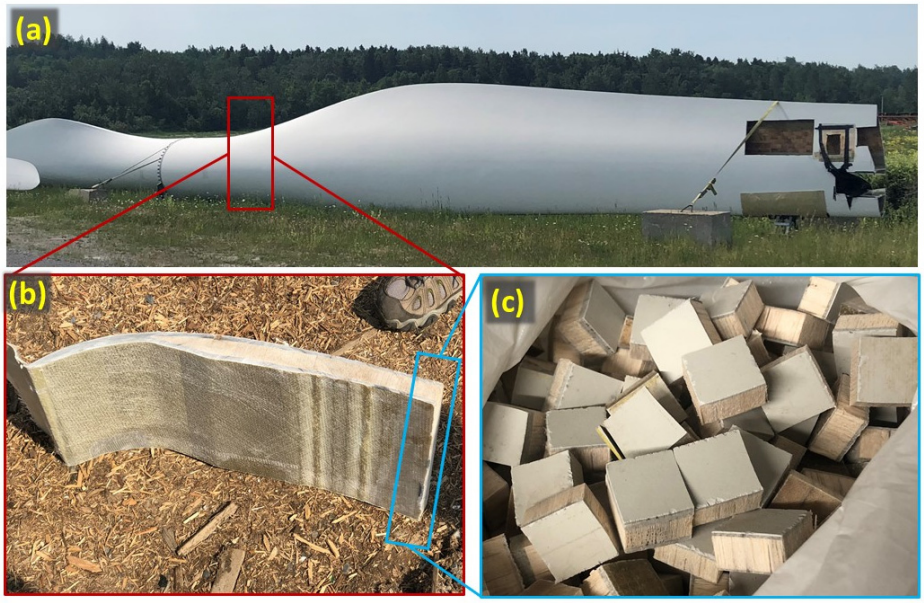

Figure 1. Waste wind-turbine blades (WWTB) material processing: (a) whole turbine blade, (b) cutting of whole turbine into smaller pieces, and (c) WWTB-GFRP aggregates.

2.1.2. Basic concrete constituents

Type General Use (GU) Portland Cement (CSA A3001) equivalent to Type I cement (ASTM C1157) [21] was used. Natural river sand (nominal maximum size of 5 mm) with a specific gravity of 2.61 and water absorption of 0.91% was also used. Crushed limestone aggregates with a specific gravity of 2.7 were considered. Natural coarse and fine aggregates fulfilling the requirements of ASTM C33 [22] were used. A nominal maximum size of 20 mm (one-fifth of the narrowest forms dimensions) was chosen according to ACI 318-19 [23] and an aggregate grade of 14 mm was added according to ASTM C192 [24]. The selection of two different grades of aggregates is aimed at increasing the packing density to achieve optimum mechanical strength. Potable water from the laboratory was used for concrete mixing. The source of water is free from any form of contamination.

2.2. Mixture proportions

To investigate the effect of GFRP-WWTB on concrete properties, two different forms of GFRP-WWTB were considered: (i) as received GFRP-WWTB after manual cutting (using the water jet saw) or grinding the chipped material into a fine powder, as well as (ii) after removal of wooden content. These two forms are termed throughout this manuscript as series WW (with wood) and series NW (no wood). For both series, GFRP-WWTB material was incorporated in replacement of cement (at rates of 0%, 10%, and 20% per cement mass) or in replacement of coarse aggregates (at rates of 0%, 50%, and 100% per volume of aggregates). These replacement levels were informed by our former investigation [12]. Table 1 presents the proportions and dry densities of concrete mixtures incorporating GFRP-WWTB (series WW and NW).

Table 1. Mixture proportions and dry densities of WWTB-GFRP concrete (kg/m^3 of concrete).

Mix Proportion	REF	Cement replacement				Aggregate replacement			
		With wood (WW)		No wood (NW)		With wood (WW)		No wood (NW)	
		10WW	20WW	10NW	20NW	50WW	100WW	50NW	100NW
Cement	410	369	328	369	328	410	410	410	410
Water	200	200	200	200	200	200	200	200	200
Sand	735	735	735	735	735	735	735	735	735
20 mm coarse aggregate	632	632	632	632	632	316	0	316	0
12 mm coarse aggregate	421	421	421	421	421	421	421	421	421
WWTB-GFRP	0	41	82	41	82	76	153	174	348
Density	2370	2257	2216	2267	2229	2059	1820	2180	2062

2.3. Specimen preparation

Specimen preparation comprised three stages: (i) preparation of GFRP-WWTB material, (ii) fabrication of GFRP confining tubes, and (iii) mixture preparation and casting.

2.3.1. GFRP-WWTB preparation

GFRP-WWTB is prepared in two forms for further testing. For cement replacement, GFRP-WWTB panels were chipped using the industrial woodchipper, followed by grinding using the ball mill (Figure 2). For aggregate replacement, GFRP-WWTB panels were manually cut into 20 mm cubes using a jet saw. For NW series, wood was manually removed from the material: wood containing cubes were put into a ball mill for a short cycle to remove wood (Figure 2g). Similarly, for powder preparation, in NW series, wood was manually removed prior to chipping and grinding in an attempt to avoid the difficulty in grinding arising from the significant divergence in hardness between wood and GFRP. Particle size distribution was measured using laser granulometry following ASTM D4464 [25]. The particle size distribution is shown in Figure 3.

Figure 2. Preparation of waste glass fiber-reinforced polymer (GFRP) material from wind-turbine blades (WWTB): (a) raw material cut into cubes for incorporation in concrete as aggregates, (b) fiber extracted from ground WWTB-GFRP, (c) removal of wooden content (for powder preparation), (d–f) preparation of WWTB-GFRP powder, and (g) wooden content removed (aggregates).

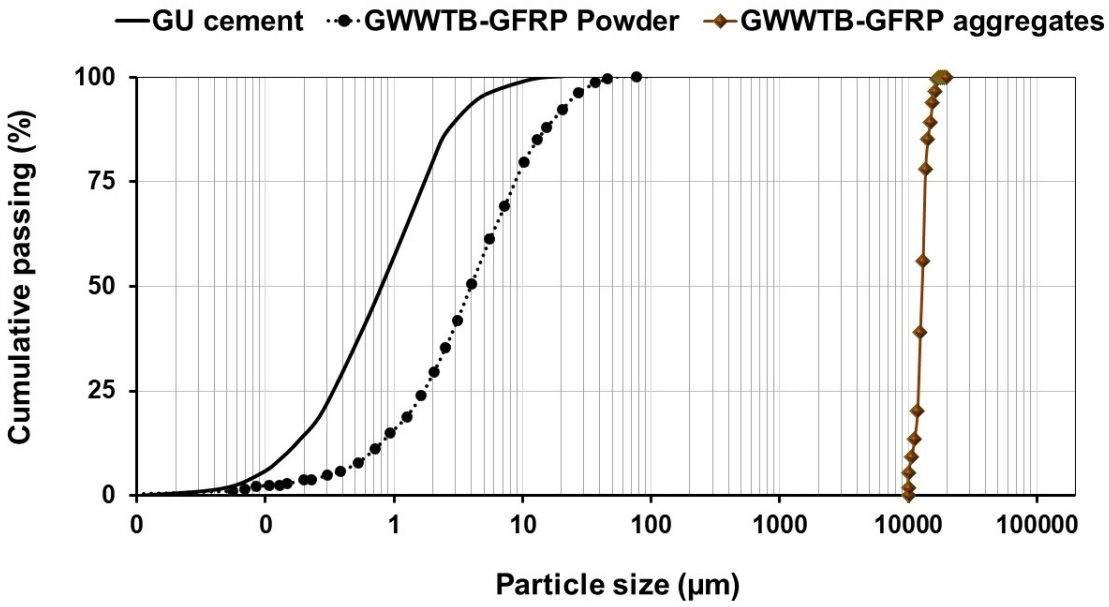

Figure 3. Particle size distribution of general use (GU) Portland cement and waste wind turbine blade GFRP (WWTB-GFRP) powder.

2.3.2. Preparation of GFRP confinement tubes

One type of circular glass fibre reinforced polymer (GFRP) tubes identical to that of El-Zefzafy et al. [20], investigated in the same research group, was considered. The tube has an inner diameter of 152 mm. The tubes were fabricated by filament winding process (Figure 4) using E-glass fibres and vinyl ester resin. Two fibres patterns were used to reinforce the tube: a helical pattern of ±65° and a circumferential pattern of 90° to increase the tube hoop strength and thus enhance the confinement efficiency. Tension and compression tests were carried out by El-Zefzafy et al. [20] on identical coupons, from the longitudinal direction, following the American standards test method ASTM D3039/D3039M [26] and ASTM D695 [27], respectively. The tension ring test was performed following ASTM D2290 [28] to determine the hoop strength. Table 2 lists the configuration and mechanical properties of the GFRP tube. After fabrication, long GFRP tubes were cut 300 mm long tubes using a circular saw. These tubes serve as stay-in-place forms for the CFFT short columns.

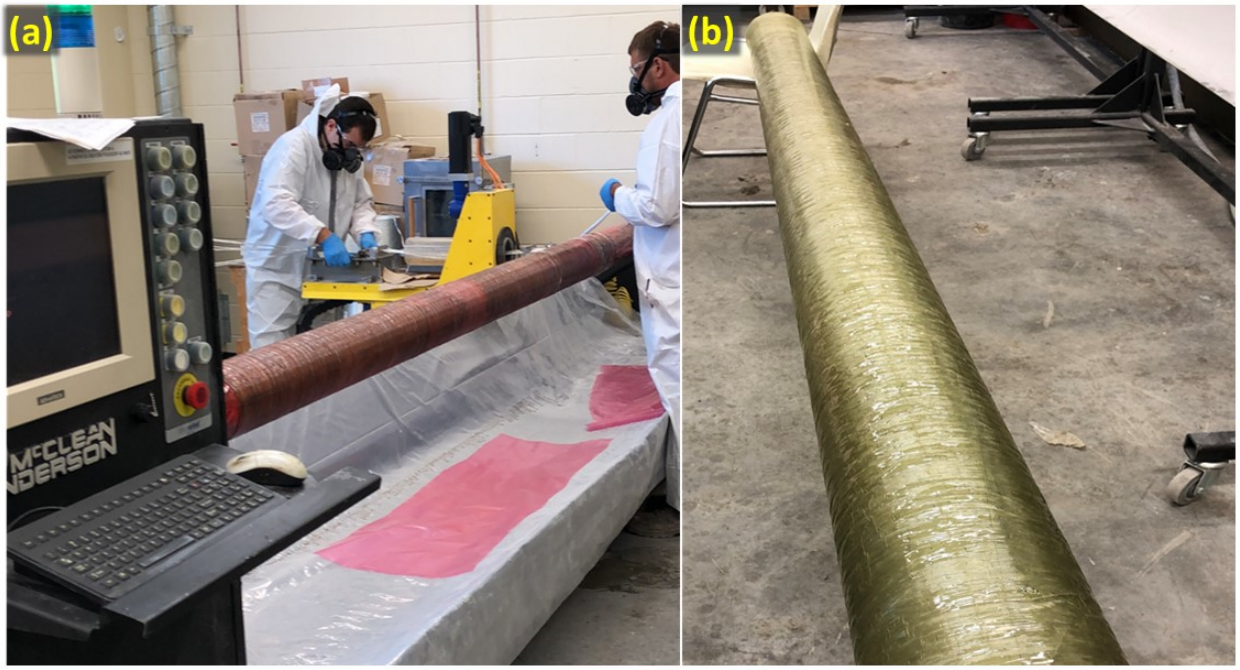

Figure 4. Fabrication of concrete-filled fibre-reinforced polymer (FRP) tubes (CFFTs): (a) filament winding setup, and (b) Final GFRP tube.

Table 2. GFRP tube configuration and mechanical properties (REF).

Diameter (mm)	Stacking sequence	No, of layers	% Fibers	Tube thickness (mm)	Mechanical properties	Axial direction			Hoop direction		
						E_{FRP} (GPa)	F_{FRP} (MPa)	ε_x (mm/mm)	E_{FRP} (GPa)	F_{FRP} (MPa)	ε_x (mm/mm)
152	(90°, ±65°, ±65°, 90°)	6	74	3.5	Tension	12	31	2.8	28.4	550	19.5
					Compression	10	−82	−8.7	-	-	-

2.3.3. Concrete mixing and sampling

Concrete batching was carried out using a 100 L capacity concrete mixer following the mixing procedure described in ASTM C192 [24]. In an attempt to enhance mixture homogeneity, GFRP-WWTB aggregates were dry-mixed with natural coarse aggregates for 10 min prior to adding them to the final mixture. After mixing, specimens were sampled for the different tests. Unconfined and confined short columns 152 × 300 mm and confined were cast. Mixtures for Series WW were cast into confined and unconfined specimens, while mixtures for Series NW were cast only into unconfined specimens (Figure 5). For each test, 3 specimens per mixture were prepared. After sampling, specimens were covered with plastic sheets and kept in a room with relative humidity (RH) and temperature of approximately 50% and 23 °C, respectively. After 24 ± 1 h, specimens were unmolded and transferred for storage in a fog room at 100% RH and 22 °C temperature until the age of testing (i.e., 28 and 90 days).

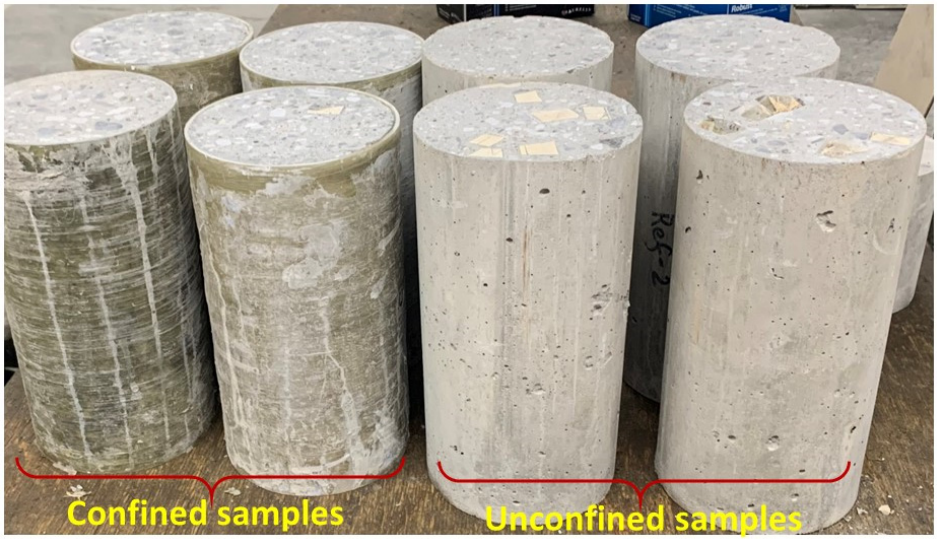

Figure 5. Test specimens: Confined (left) and unconfined (right).

2.4. Testing

2.4.1. Compressive behavior

All short columns samples were brought to room temperature before testing. The contact faces (top and bottom) were surface-polished prior to testing to ensure uniform stress distribution during testing. A 5000 kN capacity hydraulic press (MTS 810) equipped with a digital acquisition system was used (Figure 6) under a displacement-controlled mode at a rate of 1 mm/min. The compression behavior for each mixture was assessed at 28 and 91 days from the average of 3 short columns following the guidelines of ASTM 39 [29].

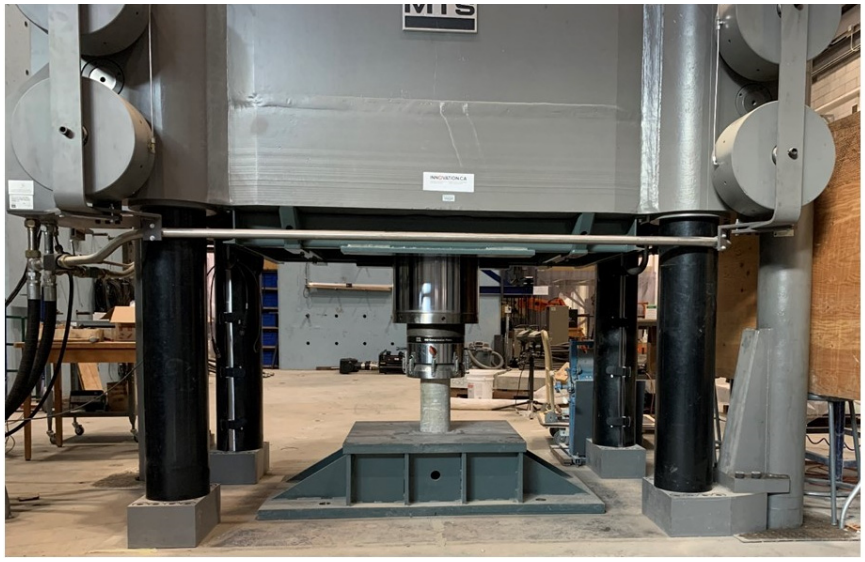

Figure 6. Test rig overview.

2.4.2. Microstructure assessment

To further understand the effect WWTB-GFRP materials on mechanical performance of concrete, a microstructure investigation using a variable pressure scanning electron microscopy (SEM) was carried to assess the effect of WWTB-GFRP aggregates on the interfacial transition zone (ITZ) with the bulk cementitious matrix following the guidelines of ASTM C1723 [30]. Polished concrete samples (with natural aggregates or WWTB-GFRP aggregates) were evaluated using a secondary electron (SE) detector operated at 15.0 kV accelerating voltage and 10 µA emission current.

3. Result analysis and discussions

The following sections discuss the results of tests performed on unconfined and confined short columns under uniaxial compression. The results are presented such that the effect of cement replacement by WWTB-GFRP powder is attempted first (section 3.1) followed by the effect of replacing natural aggregates with WWTB-GFRP aggregates (section 3.2).

3.1. Mixtures with cement replacement by WWTB-GFRP powder

3.1.1. Uniaxial compression behavior at 28 days

The effects of WWTB-GFRP powder on the uniaxial compression behavior of plain concrete and CFFT specimens at 28 days are presented in Figure 7a. The compressive strength-axial strain curves are depicted in Figure 8a and Figure 8b for unconfined specimens and in Figure 8c for CFFT confined specimens. Comparative responses between confined and unconfined short columns are also depicted in Figure 8d–f.

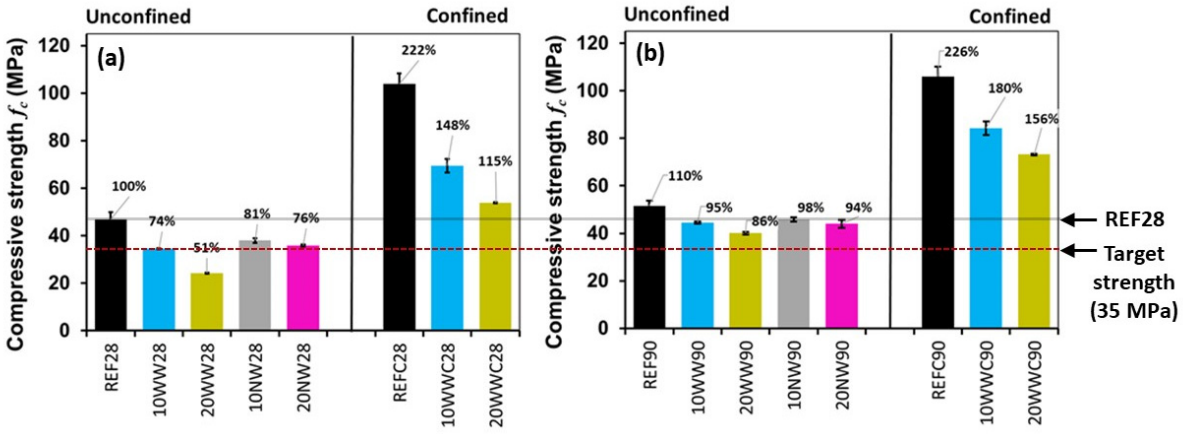

Figure 7. Compression test results for mixtures with cement replacement: (a) 28 days; (b) 90 days.

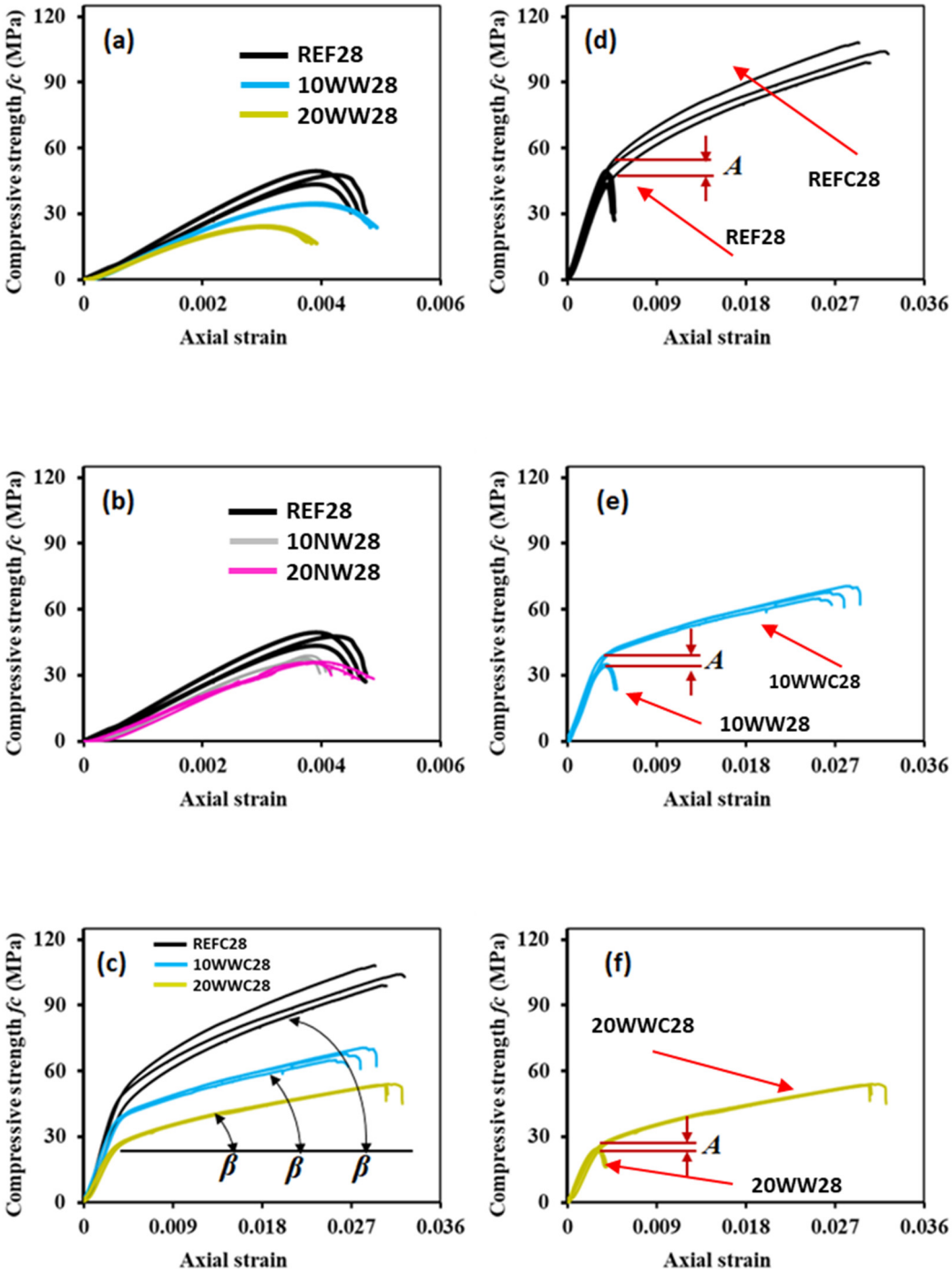

Figure 8. Compressive strength-axial strain curves for mixtures with cement replacement at 28 days: (a) With wood (WW), (b) no wood (NW), (c) with wood confined (WWC), (d) comparative response between confined and unconfined REF, (e) comparative response between confined and unconfined 10% cement replacement with Wood containing WWTB-GFRP, (f) comparative response between confined and unconfined 20% cement replacement with wood containing WWTB-GFRP aggregates; "*A*" denotes the increase the peak strength; "*β*" denotes the slope of the plastic response.

As expected, noticeable decrease in uniaxial compression resistance was observed with the increase of WWTB-GFRP powder containing wood. Strength degradation reached 49% (relative to the reference) for the mixture 20WW, which is consistent with results reported elsewhere [12]. Although WWTB-GFRP is a SiO_2-rich material, its adverse effects on strength gain shouldn't be is non-trivial. Such trend is also observed in common SiO_2-rich supplementary cementitious materials (SCMs) such as fly ash, slag, and ground glass pozzolans owing to their slow reaction and dilution effect hindering strength gain at early ages [31,32]. Such effects are attenuated at later ages as more secondary C–S–H are formed from the pozzolanic reaction as to be detailed in the subsequent section.

Additional to the dilution effect highlighted above, the retarding effect of WWTB-GFRP is further mobilized by the presence of organic content (i.e., polysaccharides in the wooden content) interfering with cement hydration kinetics and causing a delay in strength gain as well as in the mechanical properties of the end product. For this reason, mixtures without wood exhibited less strength drop than mixtures with wood where compressive strength of 81% and 76% (relative to that of the reference mix) were obtained for the mixtures 10NW and 20NW, respectively.

Interestingly, confined short columns exhibited more than 100% increase in compressive strength and more than 600% increase in axial strain compared to unconfined specimens. Confined specimens from the mixtures 10WW and 20WW exhibited a 48% and 15% increase in compressive strength compared to the unconfined reference mix. Compared to the mixtures with aggregate replacement, no significant increase in the elastic stage peak load was observed.

While a blend of dilution and retarding effect from wood component in WWTB-GFRP limit the level of cement replacement with WWTB-GFRP as demonstrated herein and elsewhere [12], it is interesting that the valorization of CFFT technology enables overcoming the strength degradation effect of WWTB-GFRP. CFFT confinement further enables higher uniaxial compression resistance ranging from 15% to 48% depending on cement replacement rate by WWTB-GFRP.

3.1.2. Compressive strength at 90 days

The effects of WWTB-GFRP powder on the uniaxial compression behavior of concrete and CFFT specimens on the 90-day strength are presented in Figure 7b. The compressive strength-axial strain curves are depicted in Figure 9a and Figure 9b for unconfined specimens and in Figure 9c for CFFT confined specimens. Comparative responses between confined and unconfined short columns are also depicted in Figure 9d–f.

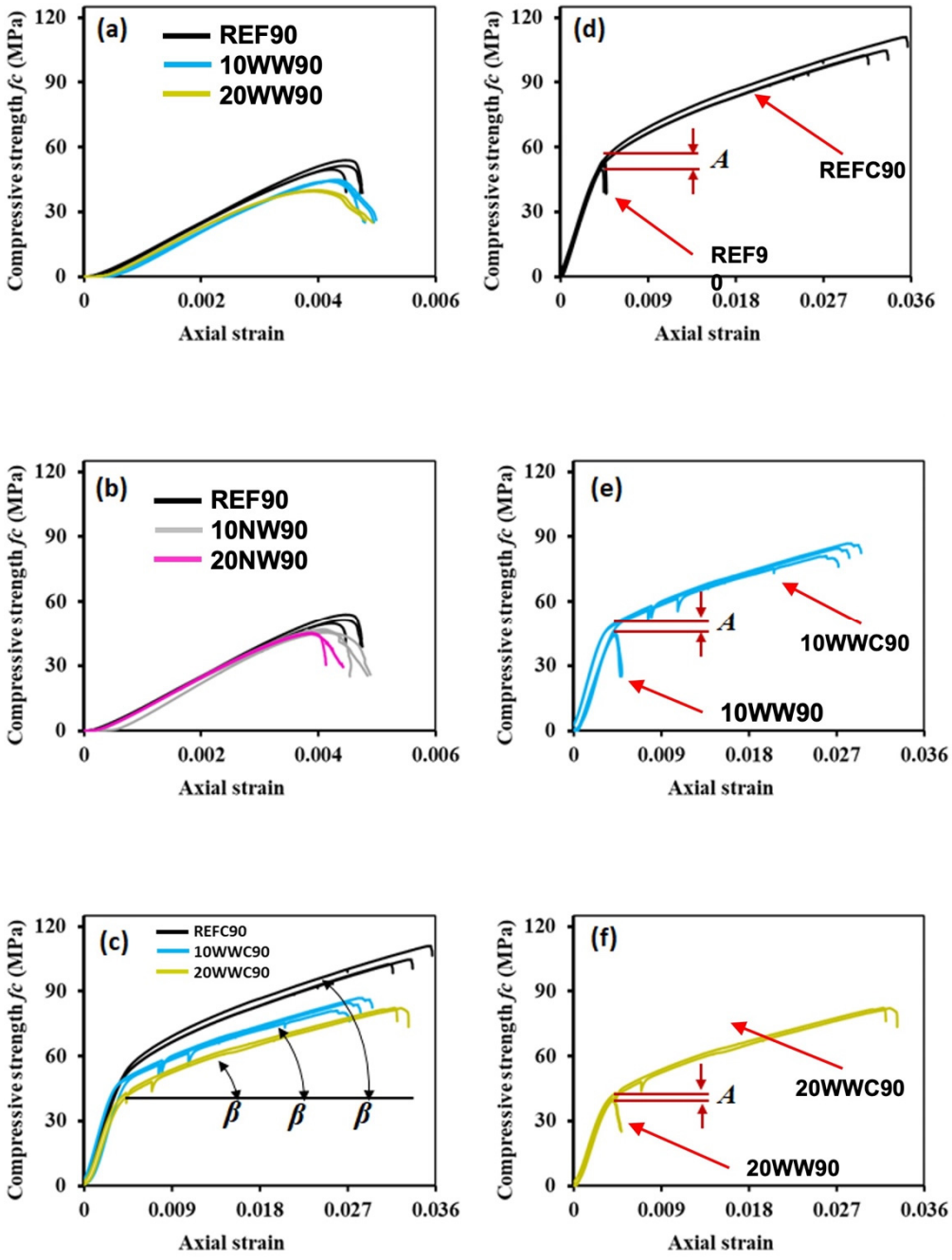

Figure 9. Compressive strength-axial strain curves for mixtures with cement replacement at 90 days: (a) With wood (WW), (b) no wood (NW), (c) with wood confined (WWC), (d) comparative response between confined and unconfined REF, (e) comparative response between confined and unconfined 10% cement replacement with Wood containing WWTB-GFRP, (f) comparative response between confined and unconfined 20% cement replacement with wood containing WWTB-GFRP aggregates; "*A*" denotes the increase the peak strength; "*β*" denotes the slope of the plastic response.

The noticeable decrease in compressive strength observed at 28 days was partially compensated for all the mixtures, with a more noticeable strength increase for mixtures containing wood. The

noticeable strength increases between 28 and 90 days can be attributed to the two mechanisms: (i) the strength gain due to the pozzolanic reaction for the powder rich in SiO_2 (for both WW and NW series), similarly to the results of [31,32], and (ii) the time-dependent depletion of the retardant effect of the wooden component (for series WW). Mixtures 10WW and 20WW attained, respectively, 95% and 86% of the strength of the reference mix at 28 days, while mixtures 10NW and 20NW attained, respectively, 98% and 94% of the strength of the reference mix at 28 days. Interestingly, with an average strength exceeding 40 MPa, all mixtures exceeded the target strength of 35 MPa sought for the chosen concrete class.

For confined specimens, the increase in compressive strength due to the confinement effect achieved 90–100% relative to the strength of unconfined samples. In general, the use of CFFTs technology shows higher effectiveness in lower strengths concrete—given that the confining effect is better mobilized when concretes incorporating high content of WWTB-GFRP exhibit lower strength and tend to split apart due to the slippery surface of the WWTB-GFRP aggregates as further detailed in section 3.2.

3.2. Mixtures with aggregate replacement

3.2.1. Compressive strength at 28 days

The effects of WWTB-GFRP aggregate on compressive strength (for unconfined and confined samples) at 28 days are presented in Figure 10a. The compressive strength versus axial strain curves for unconfined specimens are depicted in Figure 11a–c and in Figure 11d–f for CFFT-confined specimens compared with unconfined specimens from the same mixtures.

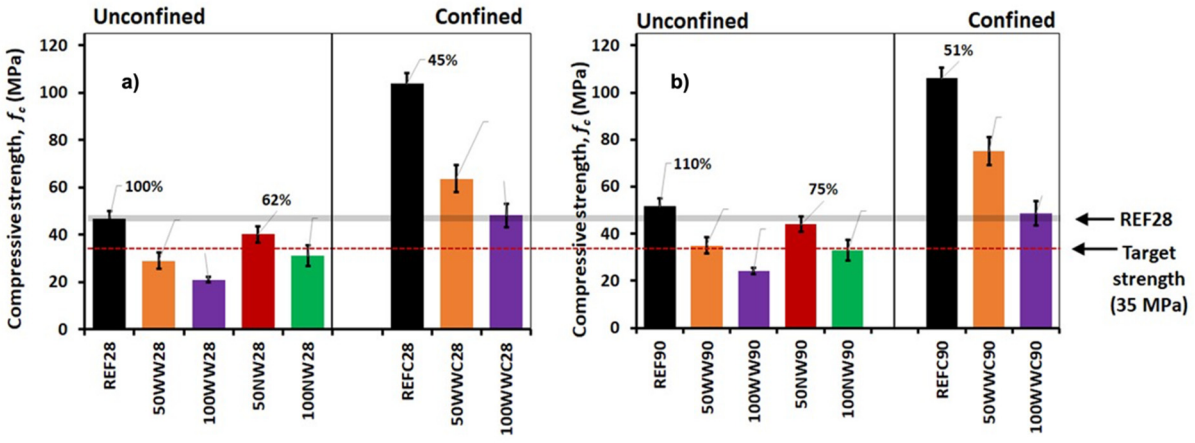

Figure 10. Compression test results for mixtures with aggregate replacement: (a) 28 days; (b) 90 days.

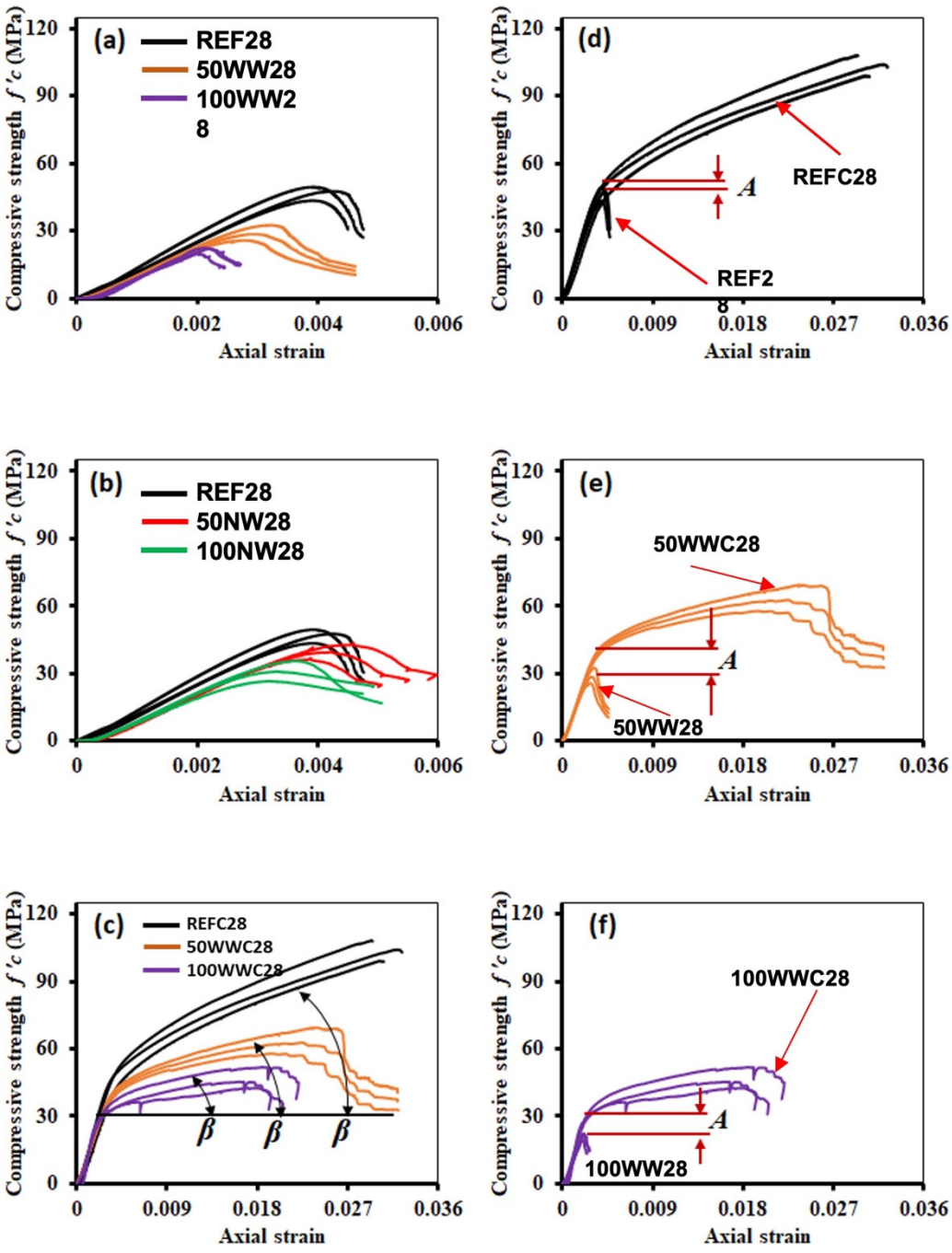

Figure 11. Compressive strength-axial strain curves for mixtures with aggregate replacement at 90 days: (a) With wood (WW), (b) no wood (NW), (c) with wood confined (WWC), (d) comparative response between confined and unconfined REF, (e) comparative response between confined and unconfined 50% aggregate replacement with Wood containing WWTB-GFRP (f) comparative response between confined and unconfined 100% aggregate replacement with wood containing WWTB-GFRP aggregates; "*A*" denotes the increase the peak strength, "*β*" denotes the slope of the plastic response.

A clear trend can be observed: the compressive strength decreases linearly for both types of aggregated (WW and NW) with increasing replacement level of aggregates as reported elsewhere [12,15]. The strength in aggregates with wood is nearly twice that for aggregates without wood. The decrease in compressive strength can be explained by two main factors: (i) lower strength WWTB aggregates (especially for the WW series), and (ii) lower frictional adhesion between the smooth WWTB-GFRP aggregate and the cementitious matrix. This leads to a lower strength in the interfacial transition zone (ITZ), known to be the weakest link in the bulk cementitious matrix as reported elsewhere [15]. Additionally, the micro-bleeding effect and the wall effect further exacerbate matrix porosity, thereby leading to decreasing the bond between cement matrix and WWTB-GFRP aggregates.

It is worth mentioning that the use of WWTB-GFRP aggregates enabled obtaining lightweight concrete. The density of concrete specimens decreased from 2370 kg/m^3 for reference mix to 2059 kg/m^3 for mixture 50WW and 1820 kg/m^3 for mixture 100WW. This allows to classify the mix 100WW as lightweight concrete according to ACI 213R-14 [33]. The compressive strength of unconfined specimens from 100WW series exceeds 17 MPa which conforms to the lightweight concrete strength criteria [33]. Confined specimens achieved up to 36% superior compressive strength compared to the reference concrete mix for 50WWC and 100WWC, while conforming to the lightweight concrete density criteria. In general, the use of CFFTs technology is more justified for the higher replacement level due to the decreased environmental impact, lower density, increase in the elastic stage peak load and acceptable compressive strength.

3.2.2. Compressive strength at 90 days

The effects of WWTB-GFRP aggregate on compressive strength of concrete and CFFT specimens on 90th day are presented in Figure 10b, the compressive strength-axial strain curves are depicted in Figure 12. The reference mix gained 10% of compressive strength between 28 and 90 days, followed by a similar strength increase for other mixes. The use of CFFT technology significantly increased the compressive strength and axial strain compared to unconfined short columns, which is consistent with 28-day results.

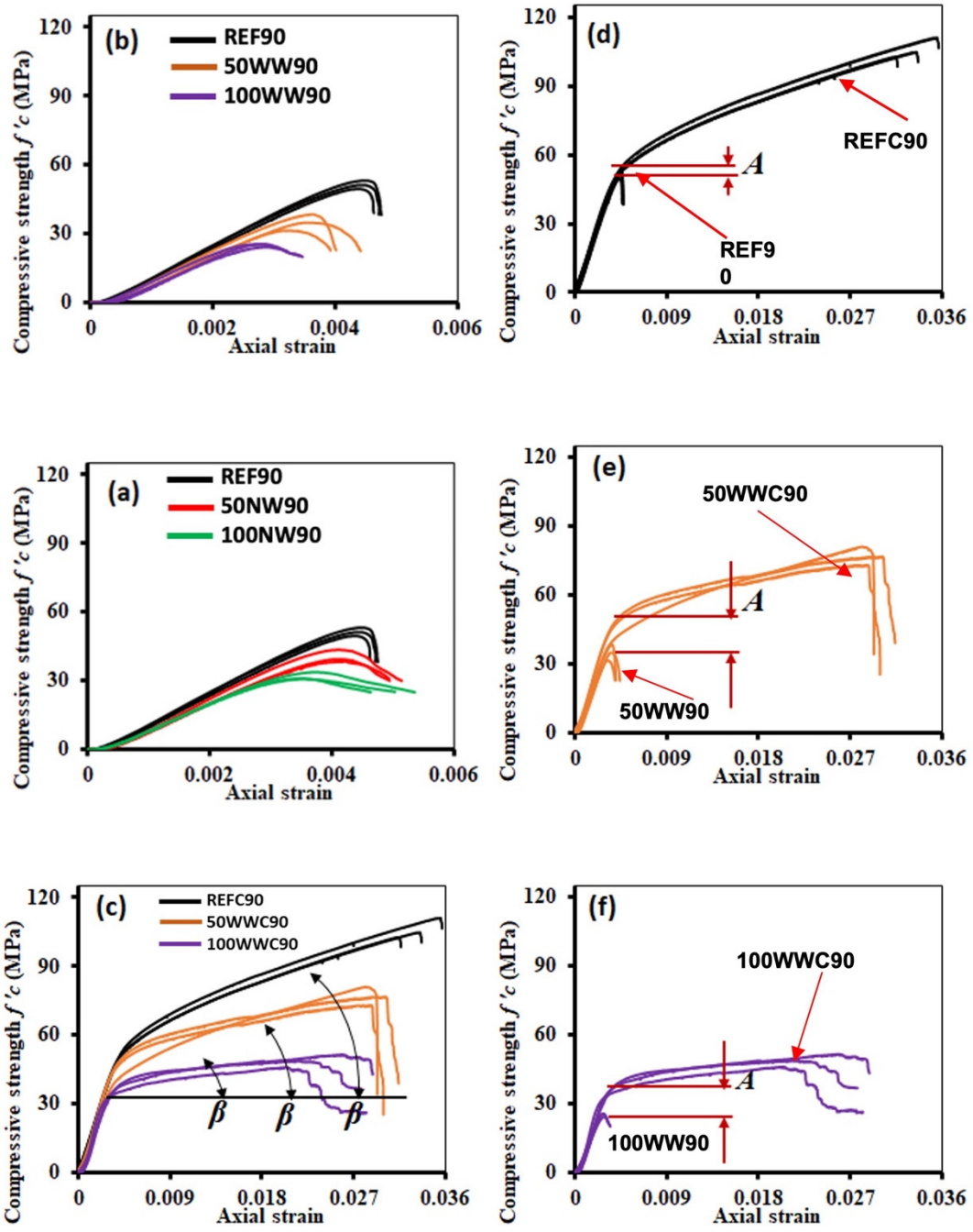

Figure 12. Compressive strength-axial strain curves for mixtures with aggregate replacement at 90 days: (a) With wood (WW), (b) no wood (NW), (c) with wood confined (WWC), (d) comparative response between confined and unconfined REF, (e) comparative response between confined and unconfined 50% aggregate replacement with wood containing WWTB-GFRP, (f) comparative response between confined and unconfined 100% aggregate replacement with wood containing WWTB-GFRP aggregates; "*A*" denotes the increase the peak strength, "*β*" denotes the slope of the plastic response.

3.2.3. Microstructure assessment of WWTB-GFRP concrete

Figure 13 presents scanning electron microscope (SEM) images at the interfacial transition zone (ITZ) between the bulk cementitious matrix and conventional aggregate (Figure 13a) as well as between the bulk cementitious matrix and WWTB-GFRP aggregates (Figure 13b). The microstructure of the ITZ in the reference concrete as depicted in Figure 13a shows a porous interfacial line between the matrix and the aggregate. Such ITZ is expected and is in alignment with former studies [34] whereby the porous interface is associated with the well reported "*wall effect*" and the "*micro-bleeding effect*" prominent at the ITZ. On the other hand, the ITZ in the concrete with 100% replacement of conventional aggregates with WWTB-GFRP aggregates shows a characteristic full-depth gap of around 300 μm separating the aggregate from the matrix—a gap that is even visible with the naked eye. This characteristic fully-gapped interface in concrete incorporating WWTB-GFRP aggregates is caused by the volumetric change in the WWTB-GFRP aggregate owing to its hydrophilic wooden content. The latter is known to swell given is water absorption propensity prior to shrinking down when concrete dries. Therefore, additional to the (i) slippery surfaces of WWTB-GFRP aggregates (at the faces with GFRP—see Figure 13b), the mechanical performance of concretes incorporating WWTB-GFRP aggregates is further influenced by (ii) the volumetric instability of WWTB-GFRP aggregates (wooden faces) which shrink as concrete dries, thereby debonding from the matrix. As a result of these two factors, WWTB-GFRP aggregates have tendency to split apart as to be discussed in section 3.2.4. These microstructure assessments further provide insights on the reasons behind strength degradation in concretes incorporating WWTB-GFRP aggregates. As such, it is not surprising that concretes with WWTB-GFRP aggregates benefited the best from CFFT-GFRP confinement when compared to concretes incorporating WWTB-GFRP powder as also elaborated further in section 3.2.4.

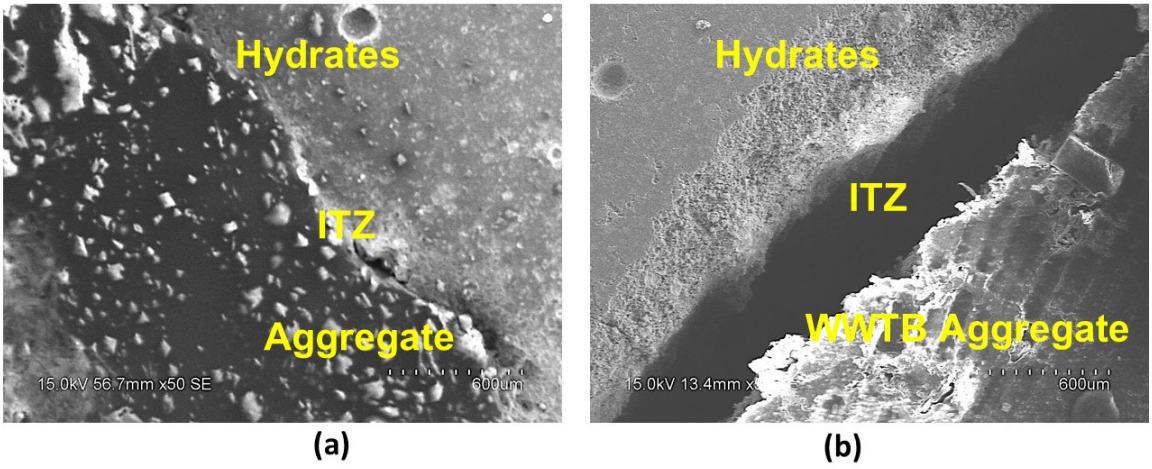

Figure 13. Scanning electron microscopy (SEM) image for the interfacial transition zone (ITZ): (a) reference concrete, and (b) concrete incorporating WWTB-GFRP aggregates. The figure shows a typical ITZ in the reference concrete as contrasted to a characteristic gap in the ITZ of WWTB-GFRP concrete due volumetric reduction in WWTB-GFRP aggregate upon drying of its hydrophilic wooden portion.

3.2.4. Effect of CFFT-GFRP confinement on compression response of WWTB-GFRP aggregate concrete

With reference to the results presented in sections 3.1.1 through 3.2.2, it is evident that the effect of CFFT confinement on compression response differs significantly from the case of cement replacement by WWTB-GFRP powder to the case of aggregate replacement by WWTB-GFRP aggregates in two perspectives. The first is the effect of confinement on the elastic response denoted by "*A*" and the second is the slope of the plastic response denoted by "*β*".

The use of CFFT technology significantly increased the compressive strength and axial strength compared to unconfined short columns. The compressive strength-axial strain curves for CFFT short columns demonstrate two distinctive regions: elastic region and plastic region, with a limited transition zone beneath, as also observed by [20]. The initial region (the elastic region) is represented by a linearly elastic slope, located close to the slope of unconfined short columns up to the ultimate unconfined strength. The following stage, the transition zone, represents the formation of the vertical cracks due to the tensile stresses in the hoop direction—Poisson's ratio effect—leading to concrete expansion in the hoop direction, thereby activating the confinement action. The transition zone is followed by the plastic stage, characterized by concrete crushing with fully activated confinement and reduced stiffness, compared to the elastic region. The curves exhibit plastic hardening behavior until the failure load. The average increase in strength and ductility was about 120% and 500%, respectively, similar to the results observed elsewhere [19].

It is important to mention the increase in elastic stage peak load and transition zone for 50WWC and 100WWC short columns (referred to as "*A*" in Figure 11e–f), representing a 14% and 28% increase compared to the unconfined short columns, respectively. This can be explained by the confining effect that provides reinforcement in the hoop direction (Figure 14) to compensate for the lack of bonding between WWTB-GFRP aggregate and the matrix. Such debonding is mobilized not only by aggregates' smooth and slippery GFRP faces, but also by the tendency of WWTB-GFRP aggregates to peel off from the matrix as a result of the interfacial gap occurring upon drying of their wooden faces—as highlighted earlier. At the plastic stage, it is worth noting that the plastic stage slope (referred to as "*β*" in Figure 11c and Figure 12c) decreases with the increase of replacement level of WWTB-GFRP aggregate. This is attributed to the reduced rigidity of WWTB-GFRP aggregates (particularly for the wooden component) compared to natural aggregates, thereby leading to a drop in the Poisson ratio effect.

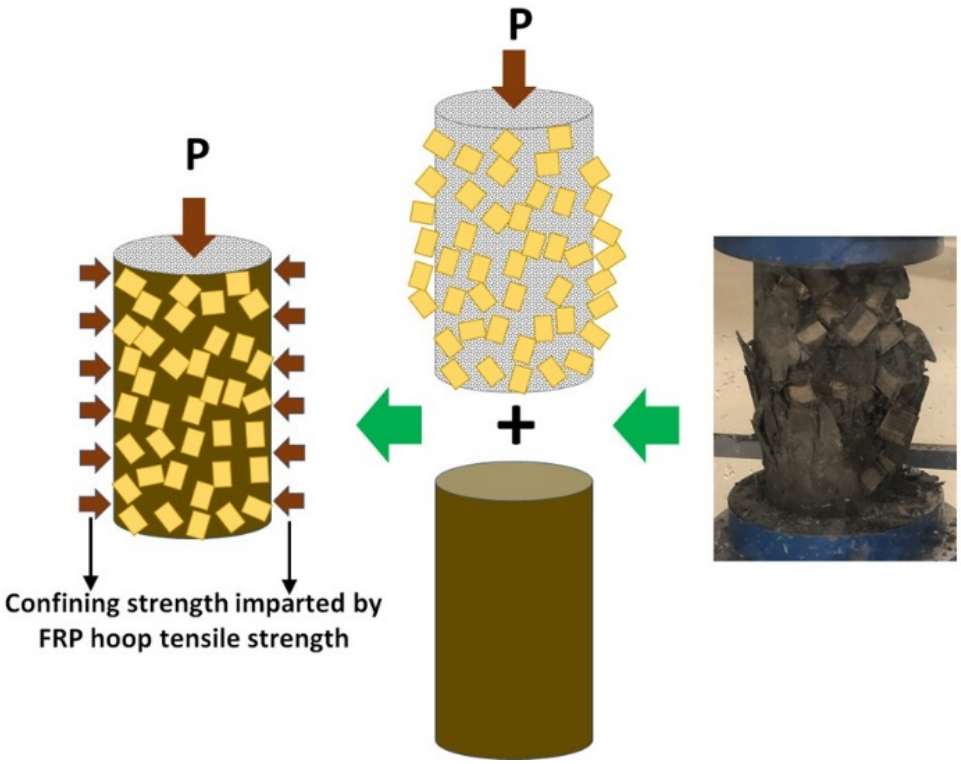

Figure 14. Confinement action of CFFTs on concrete with aggregate replacement by WWTB-GFRP.

3.2.5. Relationship between WWTB-GFRP aggregate replacement level and the compressive response

To further elucidate the effect of CFFT-GFRP confinement on enhancing the compressive response of WWTB-GFRP aggregate concrete, a simplified analytical assessment has been conducted and depicted in Figure 15. The figure shows that the level of augmentation (A) in the elastic compressive response of WWTB-GFRP aggregate concrete is linearly inked to the WWTB-GFRP aggregate replacement level (L). This linearity has been demonstrated at both 28 and 90 days with an almost perfect correlation factor (R) of 1.00. At low L values, A is almost nil. This is attributed to the fact that A strongly depends on the confinement effect preventing WWTB-GFRP aggregates from splitting due to their smooth surfaces and their gapped interfacial transition zone (ITZ) as substantiated in section 3.2.3. As L increases from 0% to 50% to 100%, A increases to more than 20% and 40%, respectively. It can also be seen that at both testing ages of 28 and 90 days, L and A are linked through the proportionality factor $C = 0.004$, which is the slope of the line. This value is characteristic to the mechanical and geometrical parameters of the confined specimen as well as its confining GFRP tube, namely, (i) concrete compressive strength (i.e., water to binder ratio), (ii) GFRP tube tensile strength, and (iii) the ratio between the GFRP tube thickness and the diameter of concrete core. As such, in the quest for higher C values to foster higher A with increasing L, future research may be directed towards optimizing the above-mentioned parameters.

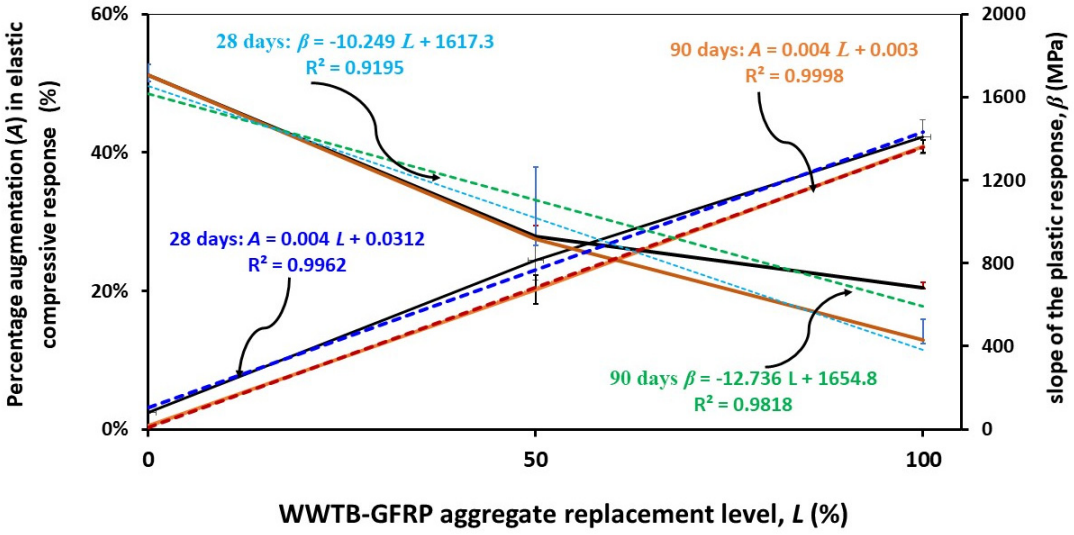

Figure 15. Relationship between WWTB-GFRP aggregate replacement level (L), percentage augmentation (A) in elastic compressive response of WWTB-GFRP aggregate concrete, slope (β) of the elastic response.

Further evidence—on the strong dependence of A on aggregate content and the opposing confining strength provided by GFRP tube to resist aggregate slippage—can be found in the analysis of the effect of confinement on the strength of concrete incorporating WWTB-GFRP powder presented in section 3.1.3. In fact, in the absence of WWTB-GFRP aggregates, it was demonstrated that while WWTB-GFRP powder significantly enhances the plastic response by increasing its slope, hence the energy absorption capacity, WWTB-GFRP powder has no effect on the elastic response.

Another factor worth consideration is the enhancement in the plastic response designated by the slope (β) of the post-peak segment. It was shown in section 3.1.3 that while cement replacement with WWTB-GFRP powder has no effect on the elastic response A, it significantly affected the slope β of the plastic response where higher WWTB-GFRP powder led to lower β due to the reduction in strength experienced at higher content of WWTB-GFRP powder. A similar trend was also confirmed in concretes incorporating WWTB-GFRP aggregates as demonstrated in Figure 15. In the figure, the descending curves show the variation in β (slope of the plastic segment) as the level of WWTB-GFRP aggregates (L) increases. At both 28 and 90 days, the relationship between β and L appears strongly linear with an R^2 of 0.90 whereby at higher L there is a clear drop in β. Interestingly, overlapping the trend of the effect of WWTB-GFRP aggregate on the elastic response (A) and the trend of the effect of WWTB-GFRP aggregate on the plastic response (β) provide a quite useful information. The two trends are opposite whereby the former (A) increases while the latter (β) deceases. As such, the two trends intersect at an optimum L value of approximately 55%. This means that, in applications necessitating lightweight concrete without stringent requirement on the plastic response, L can be pushed to its maximum limit (L = 100%) to take full advantage of WWTB-GFRP aggregates while going green. However, in applications where stability is fundamental and rigidity at post cracking is critical, L can be maintained at fairly low values to benefit from higher β. In contrast, in applications necessitating improvement in both parameters A and β, the above simplified analysis suggests that the content of WWTB-GFRP in aggregate (L) needs to be maintained at the optimum

content, within 55% for the current experimental campaign. This optimum value is experiment-sensitive and can vary depending on above mentioned factors, i.e., (i) matrix compressive strength (i.e., water to binder ratio), (ii) CFFT hoop tensile strength, and (iii) the ratio between the CFFT tube thickness and the diameter of concrete core.

3.2.6. Analytical modeling of the compressive behavior of confined WWTB-GFRP-aggregate concrete

To provide further analytical assessment of the compressive response of model WWTB-GFRP concrete in CFFT confinement, the empirically derived A and β coefficient described earlier were utilized by valorizing (and calibrating) existing stress–strain models developed by multiple researchers and adopted by the American Concrete Institute [35–38]. One of such stress–strain models is the one initially developed by Lam and Teng (2003) [38] then adopted by ACI 440.2R-17 guidelines [30]. In this model, the stress–strain curve of FRP confined concrete is represented with two curves i.e., a parabolic first curve (Eq 1) followed by linear-elastic second curve (Eq 2) with a slope E_2 (Eq 3). The parabolic curve meets the linear-elastic curve at a transition strain ε_t (Eq 4).

$$f_c = E_c\varepsilon_c - \frac{(E_c - E_2)}{4f_c^{'}}\varepsilon_c^2,\ 0 \le \varepsilon_c \le \varepsilon_t \tag{1}$$

$$f_c = f_c^{'} + E_2\varepsilon_c,\ \varepsilon_t \le \varepsilon_c \le \varepsilon_{c,max} \tag{2}$$

$$E_2 = \frac{2f_{cc}^{'} - 2f_c^{'}}{\varepsilon_{ocu}} \tag{3}$$

$$\varepsilon_t = \frac{2f_c^{'}}{(E_c - E_2)} \tag{4}$$

where $f_{cc}^{'}$ is the maximum confined concrete compressive strength, calculated as follows (Eq 5):

$$f_{cc}^{'} = f_c^{'} + \psi_f 3.3\kappa_a f_l \tag{5}$$

f_l is the maximum confinement pressure, $\psi_f = 0.95$, κ_a can be taken as 1.0 for circular cross-section (Eq 6).

$$f_l = \frac{2E_f nt\varepsilon_{fe}}{D} \tag{6}$$

where n is the number of layers of FRP jackets (n = 1 for FRP tube), t is the tube thickness. The effective strain in the FRP at failure ε_{fe} can be given by (Eq 7):

$$\varepsilon_{fe} = \kappa_\varepsilon \varepsilon_{fu} \tag{7}$$

With $\kappa_\varepsilon = 0.586$ according to Lam and Teng (2003) [38], and ε_{fu} the design rupture strain of FRP reinforcement attained at failure.

The maximum compressive strain in the FRP-confined concrete can be found as (Eq 8):

$$\varepsilon_{ccu} = \varepsilon_c^{'}\left(1.50 + 12\kappa_b \frac{f_l}{f_c}\left(\frac{\varepsilon_{fe}}{\varepsilon_c^{'}}\right)^{0.45}\right) \tag{8}$$

κ_b can be taken as 1.0 for circular cross-section, and ε_c' is the compressive strain of unconfined concrete and can be taken as 0.002.

Using the experimental data compiled in this campaign, the analytical compressive behavior predicted by ACI 440.2R-17 was plotted for the three classes of concretes tested in this experimental campaign, namely concrete with 0%, 50% and 100% aggregate replacement by WWTB-GFRP. The corresponding ACI predicted response as compared to the experimental response for the above three classes of concrete are presented in Figure 16a–c, respectively. There are two distinctive features to highlight:

First, for conventional concretes not containing WWTB-GFRP aggregates (labeled by REF in Figure 16a) it can be seen from the graphs that, with primarily the knowledge of the compressive strength of unconfined concrete (f_c'), ACI 440.2R-17 analytical model (the double line curve with square markers in Figure 16a) predicts to some extent the compressive behaviour of conventional concrete specimens, whether unconfined (REF: the red-dashed line curve) or confined (REFC: the green dashed line curve). See Figure 16a, with the remark that if we use ACI model for the unconfined case, the second segment of the curve will be omitted. Thus, ACI model can predict the behavior of conventional concrete to some extent.

However, when WWTB-GFRP aggregates are used, the ACI 440.2R-17 model can't capture well the compressive behaviour of concrete by relying solely on the compressive strength of the unconfined concrete (f_c') as we did with conventional concrete. This is due to the complex nature of concrete incorporating WWTB-GFRP aggregates, whereby their compressive failure mechanism under confinement activates the confining tensile hoop strength to counterbalance the tendency of aggregates to split du to: (i) their slippery GFRP surfaces, and (ii) the intrinsic, porous, aggregate-matrix interfacial gap caused by the drying shrinkage of the wooden faces of WWTB-GFRP aggregates, as elaborated earlier. These mechanisms behind introducing A and β to characterise the compressive behavior of concrete incorporating WWTB-GFRP aggregates

Therefore, integrating the coefficients, A and β into the ACI 440.2R-17 constitutive laws allows refining ACI model such that its predicted results are the closest to the experimental ones. By integrating A and β into Eqs 1,2,4, the modified versions of these three equations (Eqs 9–11) can be presented as:

$$f_c = E_c\varepsilon_c - \frac{(E_c-\beta)}{4f_c'(A+1)}\varepsilon_c^2,\ 0 \le \varepsilon_c \le \varepsilon_t \tag{9}$$

$$f_c = f_c'(A+1)\ + \beta\varepsilon_c,\ \varepsilon_t \le \varepsilon_c \le \varepsilon_{c,max} \tag{10}$$

$$\varepsilon_t = \frac{2f_c'(A+1)}{(E_c-\beta)} \tag{11}$$

With $E_2 = \beta$ represent the second slope of the graphs in the post-elastic portion, and (A + 1) represents the slope of the elastic portion. Notice that Eq 10 factors f_c' by a term of (A + 1) to account for the increase in f_c' contributed by the confinement effect.

Figure 16 also shows a plot of ACI 440.2R-17 model as well as the adjusted equations (termed here in as "modified"). The modified ACI 440.2R-17 model (solid dark line with circular markers in all graphs) allows higher predictability for the compressive behavior not only for concretes incorporating 50% WWTB-GFRP (Figure 16b) and 100% (Figure 16c) WWTB-GFRP, but also for the reference mixture (Figure 16a).

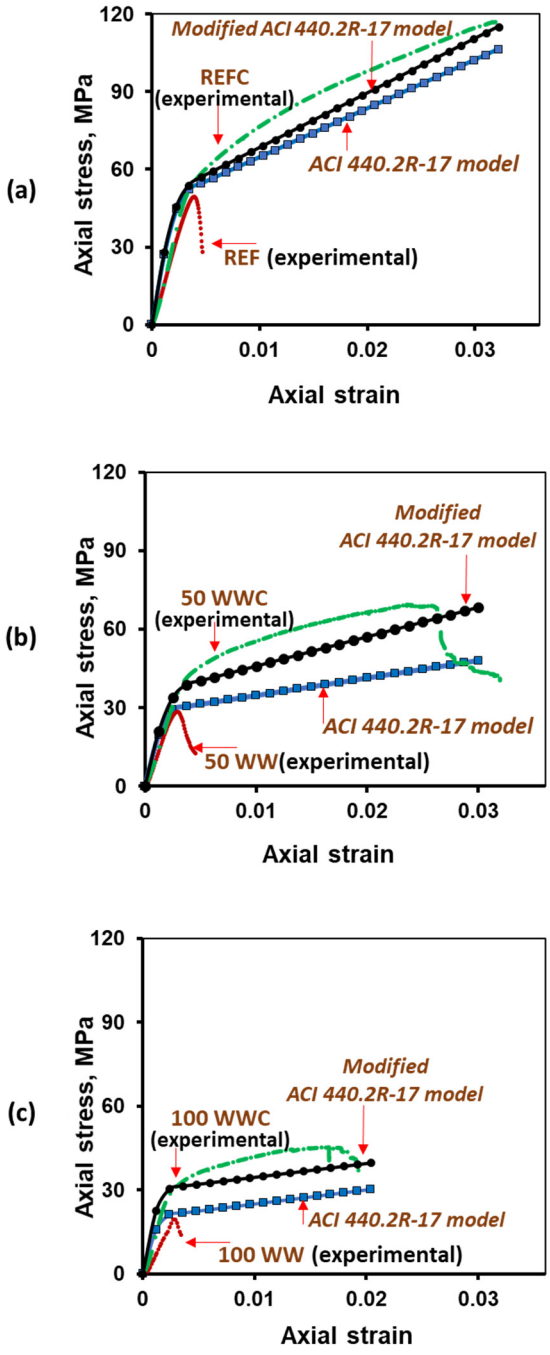

Figure 16. Experimental and analytical stress–strain curves for unconfined and confined specimens: (a) Reference concrete series REF and REFC; (b) 50WW and 50WWC series; (c) 100WW and 100WWC series.

One interesting feature of this ongoing analytical assessment is that the proposed modified ACI 440.2R-17 model can be used in conjunction with the relationship between WWTB-GFRP aggregate replacement level presented in Figure 15. In fact, knowing that A and β coefficient (that determine the compressive response of confined concrete with WWTB-GFRP aggregates) are linearly correlated to the WWTB-GFRP aggregate replacement level (L), the modified ACI 440.2R-17 model

can be used to predict the compressive behaviour of confined specimens at various replacement levels of WWTB-GFRP aggregate.

Therefore, with the knowledge of the target replacement level (L) of natural aggregates with WWTB-GFRP aggregates (say L = 55% which appears to be an optimum point for A and β, alike), one can use Figure 15 to obtain the corresponding A and β coefficients. Then, with the prior knowledge of target unconfined concrete strength (f_c'), one can integrate these parameters (f_c', A and β) in the modified ACI 440.2R-17 model to predict the compressive behavior of the corresponding WWTB-GFRP aggregate concrete.

While our results confirm that ACI 440.2R-17 model has low sensitivity to the behavior of confined concretes containing WWTB-GFRP aggregates, it should be clarified that our assessment is based on our test data, whereby A and β coefficient are governed primarily by the aggregate replacement level (L%). More extensive research at different L values while examining further factors affecting A and β can help to further calibrate the model.

4. Summary and conclusions

As summarized graphically in Figure 17, this study investigated two schemes for valorising glass fiber-reinforced polymer materials originating from disassembled wind-turbine blades (WWTB-GFRP) in concrete. WWTB-GFRP powder with wood and after wood removal (at 10–20% cement replacement), and lightweight aggregates with wood and after wood removal (at 50–100% replacement of coarse limestone aggregate) were incorporated into concrete and tested at 28 and 90 days. With reported mechanical strength loss in WWTB-GFRP concrete observed herein and elsewhere, an innovative approach was adopted herein to overcome this challenge. It consists of confining WWTB-GFRP concrete using concrete-filled fibre-reinforced polymer (FRP) tubes (CFFTs) technology. Specific findings are:

- While WWTB-GFRP powder negatively affects compressive resistance of concrete mainly due polysaccharides in the wooden content interfering with cement hydration kinetics, WWTB-GFRP aggregates adversely affected the compressive strength of concrete due to two factors: (i) the smooth surface of WWTB-GFRP aggregates leading to lower adherence and less mechanical interlocking with the matrix when compared to limestone aggregate, and (ii) the separation of WWTB-GFRP aggregates from the matrix as a result of their wooden faces shrinking as concrete dries (as microstructurally evidenced herein). Yet, upon removal of the wooden content, all mixtures incorporating WWTB-GFRP material passed—at 90 days—the target strength of 35 MPa intended for the tested grade of concrete.
- Despite the drop in mechanical strength observed with WWTB-GFRP concretes, mixes with up to 100% aggregate replacement by WWTB-GFRP incorporating wood enable obtaining formulations satisfying the requirement for lightweight concrete in terms of compressive strength (≈17 MPa) and density (≈1820 kg/m^3).
- Upon valorizing WWTB-GFRP materials suing CFFTs technology, enhancement in strength of 90–120% for both powders and aggregates (with wood and without wood, alike) was observed. CFFT confinement allowed to significantly improve the compressive strength of all mixtures. For mixtures with aggregate addition, an increase of 14% and 28% was observed for 50% and 100% replacement, respectively. For mixtures with powder addition, the increase in compressive strength of 90–100% was observed

- CFFT confinement shifted the compressive stress–strain response of WWTB-GFRP concrete from the conventional brittle response to a ductile one, whereby the confinement affected the elastic and plastic responses differently. As the replacement level of aggregates by WWTB-GFRP aggregates increased from 0 to 100%, CFFT confinement increased the elastic limit, but a lower slop of the plastic response was recorded at higher WWTB-GFRP aggregate content. An analytical assessment demonstrated that a WWTB-GFRP aggregate content of 55% will be optimum for enhancing both elastic and plastic responses while going green and lightweight.
- Building upon the ACI 440.2R-17 model for predicting the compressive response of confined concrete incorporating conventional aggregates, a modified model more sensitive to WWTB-GFRP aggregates and with higher predictive ability was proposed.
- The coupled effect of WWTB-GFRP and CFFT confinement enabled to obtain (i) a low-cement concretes exhibiting the mechanical performance of high-performance concrete (above 60 MPa) for the case of cement replacement, and (ii) a WWTB-GFRP-based lightweight concretes exhibiting the compressive strength of conventional concrete (above 35 MPa) for the case of aggregate replacement. As such, coupling the uses of WWTB-GFRP materials and CFFT conferred a threefold benefit to concrete materials: (i) lightweight (supported by FRP's reduced density), (ii) strength (supported by the CFT confinement shifting the failure from the traditional brittle one to a more ductile one), and (iii) sustainability (supported by cement and aggregate replacement by an otherwise waste material).

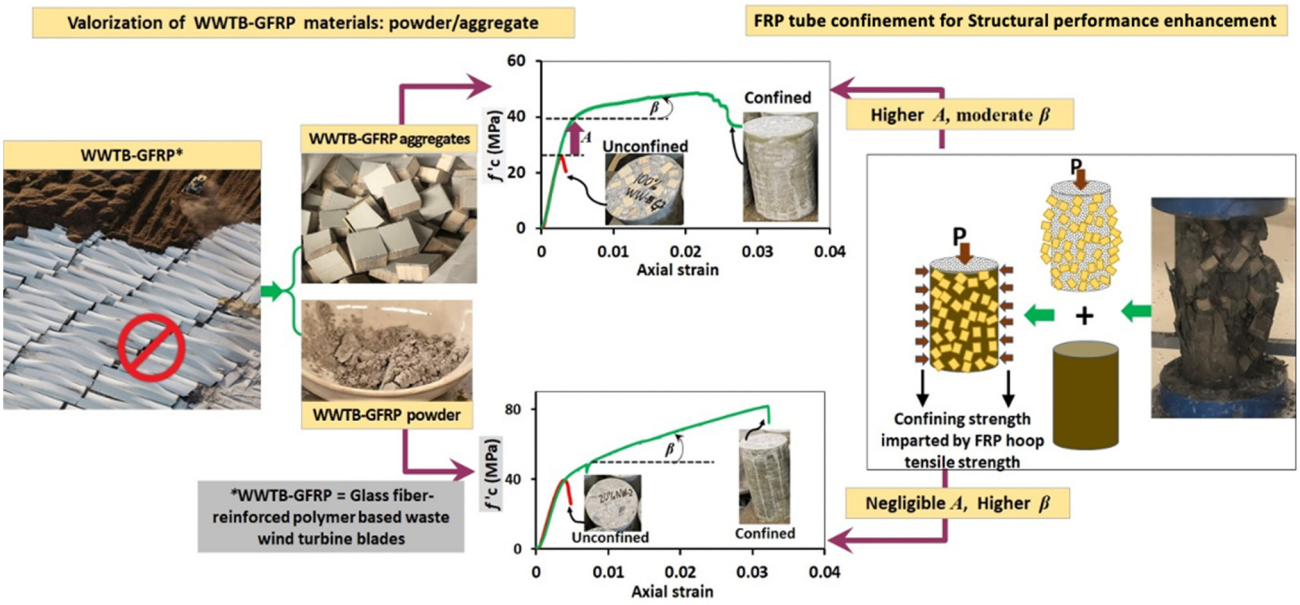

Figure 17. Summary of research methodology and outcomes.

Overall, CFFT confinement of WWTB-GFRP concretes enables restoring the strength loss and taking benefit of this sustainable alternative while fostering a higher strength to weight ratio given the lightweight concretes obtained. Low-cement and low-natural aggregate concretes with equal or superior strength compared to conventional concretes can be obtained using the combination of WWTB-GFRP with CFFT technology. Thus, it can be concluded that WWTB-GFRP is a promising material for valorization in concrete construction to enable the transition to carbon neutrality in the

cement and concrete sector while promoting the sustainable development through offering a second life to waste materials.

Acknowledgements

The authors wish to acknowledge the financial support of the Natural Sciences and Engineering Research Council of Canada and Québec Research Funds for Nature and Technology (FRQNT). Special thanks to the Groupe Bouffard and LM-Wind Power for their collaboration in conducting this study. The assistance of the technical staff of the Structural and Materials Laboratory in the Civil & Building Engineering Department at the University of Sherbrooke is also greatly appreciated.

Conflict of interest

The authors declare no conflict of interest.

References

1. GWEC, Global Wind Report Annual Market Update 2015. Global Wind Energy Council, 2015. Available form: https://www.gwec.net/wp-content/uploads/vip/GWEC-Global-Wind-2015-Report_April-2016_22_04.pdf.
2. Beauson J, Brøndsted P (2016) Wind turbine blades: An end of life perspective, In: Ostachowicz W, McGugan M, Schröder-Hinrichs JU, et al., *MARE-WINT New Materials and Reliability in Offshore Wind Turbine Technology*, Cham: Springer Nature, 421–432. https://doi.org/10.1007/978-3-319-39095-6_23
3. European Council, Conclusions on 2030 Climate and Energy Policy Framework. Council of the EU, 2014. Available form: http://www.consilium.europa.eu/en/press/press-releases/2014/10/pdf/European-Council-%2823-and-24-October-2014%29-Conclusions-on-2030-Climate-and-Energy-Policy-Framework/.
4. Canadian Renewable Energy Association, Wind Energy. Canadian Wind Energy Association, 2021. Available form: https://canwea.ca/wind-facts/why-wind-works/.
5. Fox T (2016) Recycling wind turbine blade composite material as aggregate in concrete [Master's thesis]. Iowa State University, United States.
6. Nagle AJ, Delaney EL, Bank LC, et al. (2020) A Comparative Life Cycle Assessment between landfilling and Co-Processing of waste from decommissioned Irish wind turbine blades. *J Cleaner Prod* 277: 123321. https://doi.org/10.1016/j.jclepro.2020.123321
7. D'Souza N, Gbegbaje-Das E, Shonfield P (2011) *Life Cycle Assessment of Electricity Production from a Vestas V112 Turbine Wind Plant*, Copenhagen: Vestas Wind Systems A/S.
8. Meira Castro AC, Carvalho JP, Ribeiro MCS, et al. (2014) An integrated recycling approach for GFRP pultrusion wastes: Recycling and reuse assessment into new composite materials using Fuzzy Boolean Nets. *J Cleaner Prod* 66: 420–430. https://doi.org/10.1016/j.jclepro.2013.10.030
9. Correia JR, Almeida NM, Figueira JR (2011) Recycling of FRP composites: reusing fine GFRP waste in concrete mixtures. *J Cleaner Prod* 19: 1745–1753. https://doi.org/10.1016/j.jclepro.2011.05.018

10. Asokan P, Osmani M, Price A (2010) Improvement of the mechanical properties of glass fibre reinforced plastic waste powder filled concrete. *Constr Build Mater* 24: 448–460. https://doi.org/10.1016/j.conbuildmat.2009.10.017
11. Asokan P, Osmani M, Price ADF (2009) Assessing the recycling potential of glass fibre reinforced plastic waste in concrete and cement composites. *J Cleaner Prod* 17: 821–829. https://doi.org/10.1016/j.jclepro.2008.12.004
12. Baturkin D, Hisseine OA, Masmoudi R, et al. (2021) Valorization of recycled FRP materials from wind turbine blades in concrete. *Resour Conserv Recy* 174: 105807. https://doi.org/10.1016/j.resconrec.2021.105807
13. Oliveira PS, Antunes MLP, da Cruz NC, et al. (2020) Use of waste collected from wind turbine blade production as an eco-friendly ingredient in mortars for civil construction. *J Cleaner Prod* 274: 122948. https://doi.org/10.1016/j.jclepro.2020.122948
14. Limbachiya MC (2004) Performance of recycled aggregate concrete, *RILEM International Symposium on Environment-Conscious Materials and Systems for Sustainable Development*, 127–136. https://doi.org/10.1617/2912143640.015
15. Hofmeister M (2012) Recycling turbine blade composites: Concrete aggregate and reinforcement, *Wind Energy Science, Engineering and Policy Undergraduate Research Symposium Proceedings*, 9/1–9/8.
16. Boumarafi A, Abouzied A, Masmoudi R (2015) Harsh environments effects on the axial behaviour of circular concrete-filled fibre reinforced-polymer (FRP) tubes. *Compos Part B-Eng* 83: 81–87. https://doi.org/10.1016/j.compositesb.2015.08.054
17. Abouzied A, Masmoudi R (2017) Flexural behavior of rectangular FRP-tubes filled with reinforced concrete: Experimental and theoretical studies. *Eng Struct* 133: 59–73. https://doi.org/10.1016/j.engstruct.2016.12.010
18. Mohamed H, Masmoudi R (2008) Compressive behavior of reinforced concrete-filled FRP tubes. *American Concrete Institute (ACI) Special Publications, SP-257–06, ACI, Farmington Hills, Mich*, 91–108.
19. Mohamed HM, Masmoudi R (2010) Axial load capacity of concrete-filled FRP tube columns: Experimental versus theoretical predictions. *J Compos Constr* 14: 231–243. https://doi.org/10.1061/(ASCE)CC.1943-5614.0000066
20. El-Zefzafy H, Mohamed HM, Masmoudi R (2013) Evaluation effects of the short-and long-term freeze-thaw exposure on the axial behavior of concrete-filled glass fiber-reinforced-polymer tubes. *J Compos* 2013: 340672. https://doi.org/10.1155/2013/340672
21. ASTM C1157/C1157M-20a, Standard Performance Specification for Hydraulic Cement. ASTM International, 2021. Available from: https://www.astm.org/c1157_c1157m-20a.html.
22. ASTM C33/C33M-11, Standard Specification for Concrete Aggregates. ASTM International, 2011. Available from: https://www.astm.org/c0033_c0033m-11.html.
23. ACI 318-19, Building Code Requirements for Structural Concrete (ACI 318-19) and Commentary. ACI Committee, 2019. Available from: https://www.concrete.org/publications/internationalconcreteabstractsportal.aspx?m=details&ID=51716937.
24. ASTM C192/C192M-19, Standard Practice for Making and Curing Concrete Test Specimens in the Laboratory. ASTM International, 2016. Available from: https://www.astm.org/c0192_c0192m-19.html.

25. ASTM D4464-15, Standard Test Method for Particle Size Distribution of Catalytic Materials by Laser Light Scattering. ASTM International, 2020. Available from: https://www.astm.org/d4464-15r20.html.
26. ASTM D3039/D3039M-17, Standard Test Method for Tensile Properties of Polymer Matrix Composite Materials. ASTM International, 2017. Available from: https://www.astm.org/d3039_d3039m-17.html.
27. ASTM D695-15, Standard Test Method for Compressive Properties of Rigid Plastics. ASTM International, 2016. Available from: https://www.astm.org/d0695-15.html.
28. ASTM D2290-19a, Standard Test Method for Apparent Hoop Tensile Strength of Plastic or Reinforced Plastic Pipe. ASTM International, 2019. Available from: https://www.astm.org/Standards/D2290.htm.
29. ASTM C39/C39M-16, Standard Test Method for Compressive Strength of Cylindrical Concrete Specimens. ASTM International, 2016. Available from: https://www.astm.org/c0039_c0039m-16.html.
30. ACI PRC-440.2-17, Guide for the Design and Construction of Externally Bonded FRP Systems for Strengthening Concrete Structures. ACI Committee 440, 2017. Available from: https://www.concrete.org/store/productdetail.aspx?ItemID=440217&Language=English&Units=US_AND_METRIC.
31. Faella C, Lima C, Martinelli E, et al. (2016) Mechanical and durability performance of sustainable structural concretes: An experimental study. *Cem Concr Compos* 71: 85–96. https://doi.org/10.1016/j.cemconcomp.2016.05.009
32. Lima C, Caggiano A, Faella C, et al. (2013) Physical properties and mechanical behaviour of concrete made with recycled aggregates and fly ash. *Constr Build Mater* 47: 547–559. https://doi.org/10.1016/j.conbuildmat.2013.04.051
33. ACI 213R-14, Guide for Structural Lightweight-Aggregate Concrete. ACI Committee 213, 2014. Available from: https://www.concrete.org/store/productdetail.aspx?ItemID=21314&Language=English&Units=US_AND_METRIC.
34. Hisseine OA, Omran AF, Tagnit-Hamou A (2018) Influence of cellulose filaments on cement paste and concrete. *J Mater Civil Eng* 30: 04018109. https://doi.org/10.1061/(ASCE)MT.1943-5533.0002287
35. Jiang T, Teng JG (2007) Analysis-oriented stress–strain models for FRP-confined concrete. *Eng Struct* 29: 2968–2986. https://doi.org/10.1016/j.engstruct.2007.01.010
36. Yang JQ, Feng P (2020) Analysis-oriented models for FRP-confined concrete: 3D interpretation and general methodology. *Eng Struct* 216: 110749. https://doi.org/10.1016/j.engstruct.2020.110749
37. Kwan AKH, Dong CX, Ho JCM (2015) Axial and lateral stress–strain model for FRP confined concrete. *Eng Struct* 99: 285–295. https://doi.org/10.1016/j.engstruct.2015.04.046
38. Lam L, Teng JG (2003) Design-oriented stress–strain model for FRP-confined concrete. *Constr Build Mater* 17: 471–489. https://doi.org/10.1016/S0950-0618(03)00045-X

AIMS Press